

## LETTER TO THE EDITOR

# Pre-supernova O-C shell mergers could produce more $^{44}\text{Ti}$ than the explosion

J. Issa<sup>1,2</sup> and F. Herwig<sup>1,2</sup>

<sup>1</sup> Astronomy Research Centre, Department of Physics & Astronomy, University of Victoria, V8P 5C2, Victoria, Canada  
e-mail: [joshuaissa@uvic.ca](mailto:joshuaissa@uvic.ca)

<sup>2</sup> NuGrid Collaboration, <http://www.nugridstars.org>

Received December 19, 2025

## ABSTRACT

**Context.** The formation of  $^{44}\text{Ti}$  in massive stars is thought to occur during explosive nucleosynthesis, however recent studies have shown it can be produced during O-C shell mergers prior to core collapse.

**Aims.** We investigate how mixing according to 3D macro physics derived from hydrodynamic simulations impacts the pre-supernova O-C shell merger nucleosynthesis and if it can dominate the explosive supernova production of  $^{44}\text{Ti}$  and other radioactive isotopes.

**Methods.** We compare a range of observations and models of explosive  $^{44}\text{Ti}$  yields to pre-explosive multi-zone mixing-burning nucleosynthesis simulations of an O-C shell merger in a  $15 \text{ M}_\odot$  stellar model with mixing conditions corresponding to different 3D hydro mixing scenarios.

**Results.** Radioactive species produced in the O shell have a spread in their pre-explosive yields predictions across different 3D mixing scenarios of 2.14 dex on average.  $^{44}\text{Ti}$  has the largest spread of 4.78 dex. The pre-explosive production of  $^{44}\text{Ti}$  can be larger than the production of all massive star models in the NuGrid data set where  $^{44}\text{Ti}$  is dominated by the explosive nucleosynthesis contribution, as well all other massive star and supernova models.

**Conclusions.** We conclude that quantitative predictions of  $^{44}\text{Ti}$  and other radioactive species more broadly require an understanding of the 3D hydrodynamic mixing conditions present during the O-C shell merger.

**Key words.** convection – nuclear reactions, nucleosynthesis, abundances – stars: massive – stars: interiors – supernovae: general

## 1. Introduction

The radioactive isotope  $^{44}\text{Ti}$  is a key tracer of explosive nucleosynthesis in core collapse supernovae (CCSN). It is primarily synthesized during  $\alpha$ -rich freeze-out from nuclear statistical equilibrium in the innermost ejecta associated with explosive Si burning by the reactions  $^{40}\text{Ca}(\alpha, \gamma)$  and  $^{43}\text{Sc}(p, \gamma)$  (Woosley & Weaver 1995; The et al. 2006; Magkotsios et al. 2010; Sieverding et al. 2023). It is observed by the emission lines 67.87, 78.32, and 1157 keV from the decay chain  $^{44}\text{Ti} \rightarrow ^{44}\text{Sc} \rightarrow ^{44}\text{Ca}$  in supernova remnants (Iyudin et al. 1994; Grebenev et al. 2012; Boggs et al. 2015; Grefenstette et al. 2014, 2017).

Recently it has been shown that  $^{44}\text{Ti}$  can be significantly produced prior to the explosion during an O-C shell merger in massive stars (Robert et al. 2025). Mergers occur a few hours prior to the CCSN of a red supergiant, therefore  $^{44}\text{Ti}$  ( $t_{1/2} = 59.1$  yr) synthesized in this event can contribute to the observed signal seen in supernova remnants. This may be the case for Cassiopeia A, as observations of its Si, Ne, Cl, and P have recently been interpreted as signatures of an O-C shell merger prior to collapse (Sato et al. 2025; Audard et al. 2025).

Cassiopeia A (Iyudin et al. 1994; Grefenstette et al. 2014, 2017) and SN 1987A (Grebenev et al. 2012; Boggs et al. 2015) both have asymmetric and clumpy distributions of  $^{44}\text{Ti}$ . This may be a signature of the pre-

explosive origin of  $^{44}\text{Ti}$  in an O- $^{12}\text{C}$  shell merger, as 3D hydrodynamic simulations show mergers have asymmetric and large-scale non-radial flows whose features could be preserved in the remnant (Andrassy et al. 2020; Yadav et al. 2020; Rizzuti et al. 2024; Sato et al. 2025). Nucleosynthesis during mergers in these 3D macro physical flows diverges significantly from 1D stellar evolution predictions in the O shell (Yadav et al. 2020; Rizzuti et al. 2024; Issa et al. 2025a,b).

In this study, we explore how pre-explosive nucleosynthesis of  $^{44}\text{Ti}$  and other radioactive isotopes depend on the mixing conditions during an O-C shell merger as motivated by 3D hydrodynamic simulations. This Letter is organized as follows: §2 provides an overview of the post-processed O-C shell conditions, §3 demonstrates how  $^{44}\text{Ti}$  is produced non-explosively and compares the production in the O-C shell merger to explosive yields, and finally in §4 we discuss the implications of these results for observations.

## 2. Methods

The NuGrid data set includes massive star models with initial masses  $12\text{--}25 \text{ M}_\odot$  and initial metallicities  $Z = 10^{-4}$  to 0.02 (Ritter et al. 2018). These models were calculated in 1D using **MESA** (Paxton et al. 2010) without rotation and no convective overshooting after the end of core helium burning (Pignatari et al. 2016; Ritter et al. 2018). Four mod-

els have an O-C shell merger shortly before core collapse:  $15 M_{\odot}$ ,  $Z = 0.02$ ,  $12 M_{\odot}$ ,  $Z = 0.01$ ,  $15 M_{\odot}$ ,  $Z = 0.01$ , and  $20 M_{\odot}$ ,  $Z = 0.02$ .

We have post-processed the O shell of the  $15 M_{\odot}$ ,  $Z = 0.02$  NuGrid multi-zone code `mppnp` (Pignatari et al. 2016) to study how nucleosynthesis of the light odd-Z isotopes and  $p$  nuclei are changed by 3D-inspired mixing scenarios (Issa et al. 2025a,b). This stellar model produces a number of radioactive species in the O-C merger prior to the explosion as shown in Fig. 1.

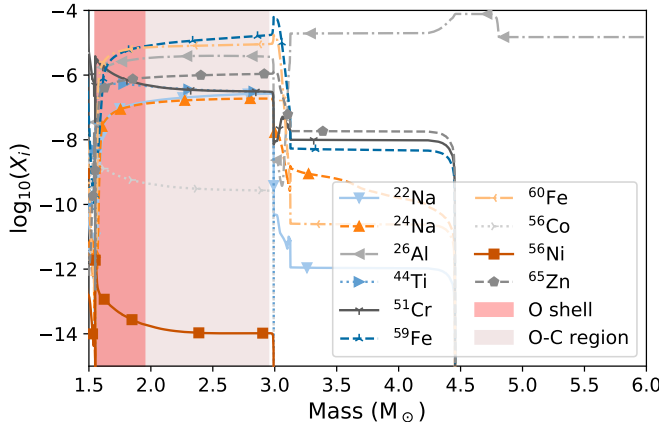


**Fig. 1.** Mass fractions of radioactive isotopes in the  $15 M_{\odot}$ ,  $Z = 0.02$  model from Ritter et al. (2018) at the final time step before explosion. Both the O shell and O-C region are shaded to indicate their extent.

The mixing scenarios inspired by 3D hydrodynamic simulations (Figures 4 and 5, Issa et al. 2025a) include a downturn in the mixing efficiency profile at the bottom of the O shell (Meakin & Arnett 2006; Jones et al. 2017), increased convective velocities compared to mixing length theory (MLT) of factors 3, 10, and 50 (a range seen in the simulations of Jones et al. 2017; Andrassy et al. 2020; Rizzuti et al. 2024), and quenching effects due to possibly strong energy feedback and partial merging (Andrassy et al. 2020). They also have a range of C-shell entrainment rates into the O shell from no entrainment to a full merger of the convective O and C shells, as the simulations of Andrassy et al. (2020) show that entrainment depends on the luminosity of  $^{12}\text{C} + ^{12}\text{C}$  burning.

We provide results in terms of an overproduction factor defined as

$$\text{OP}_{\text{R15}} = X_{\text{model}} / X_{\text{Pre-Explosive } 15 M_{\odot}, Z=0.02}$$

where  $X_{\text{model}}$  is the ejected yield for a species from a given model and  $X_{\text{Pre-Explosive } 15 M_{\odot}, Z=0.02}$  is the undecayed pre-explosive yield from the  $15 M_{\odot}$ ,  $Z = 0.02$  model from Ritter et al. (2018). The simulations from Issa et al. (2025a,b) simulate the O shell alone for 110 s, and so the yields for these models are estimated according to the method described by §2.3 of Issa et al. (2025b). Further simulation details can be found in Issa et al. (2025a,b).

### 3. Results

#### 3.1. Nuclear production of $^{44}\text{Ti}$ during O-C shell mergers

All mixing cases considered in this work share a single, common reaction chain that produces  $^{44}\text{Ti}$  during the O-C

shell merger:  $^{38}\text{Ar}(\alpha, \gamma)^{42}\text{Ca}(n, \gamma)^{43}\text{Ca}(p, \gamma)^{44}\text{Sc}(p, n)^{44}\text{Ti}$ . The importance of  $^{44}\text{Sc}$  is not seen in explosive nucleosynthesis, but it is clearly shown in Fig. 2 for our pre-explosive conditions. All mixing conditions also share  $^{44}\text{Ti}(\gamma, \alpha)^{40}\text{Ca}$  as the dominant destruction channel at the base of the shell where  $T = 2.77 - 2.83 \times 10^9$  K.  $^{44}\text{Ti}(n, \gamma)^{45}\text{Ti}$  is also a destruction channel, but to a lesser extent.

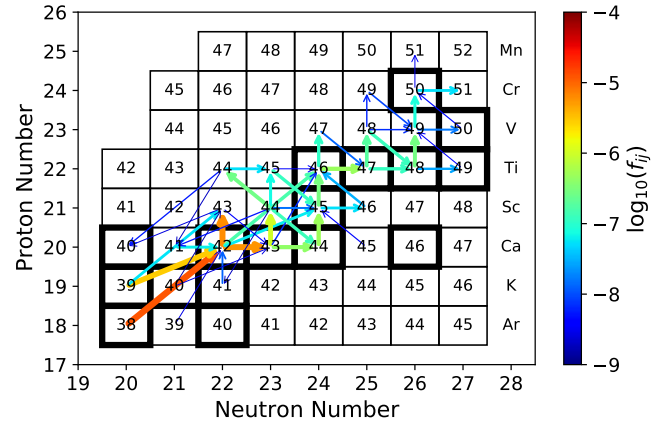


**Fig. 2.** Chart of reactions between isotopes at  $m = 1.6 M_{\odot}$  [ $T = 2.494 \times 10^9$  K] for the  $50 \times D_{\text{3D-insp.}}$  mixing case with an ingestion rate of  $4 \times 10^{-3} M_{\odot}\text{s}^{-1}$  at  $t = 110$  s. Both arrow colour and size indicate  $\log_{10}(f_{ij})$ , the reaction flux as defined in Issa et al. (2025a), and arrows point in the direction of the reaction.

The mixing cases with a  $50 \times D_{\text{3D-insp.}}$  profile have some exceptions to the  $^{38}\text{Ar}$  and  $^{42}\text{Ca}$  contributions to  $^{44}\text{Ti}$ . These cases feature significant contributions of  $^{39}\text{K}(\alpha, p)^{42}\text{Ca}$  and  $^{43}\text{Sc}(\gamma, p)^{42}\text{Ca}$  along with  $^{38}\text{Ar}(\alpha, \gamma)^{42}\text{Ca}$ . The contribution of  $^{43}\text{Sc}$  to  $^{42}\text{Ca}$  may seem counter-intuitive as Fig. 2 shows  $^{42}\text{Ca}(p, \gamma)^{43}\text{Sc}$  as a destruction channel for  $^{42}\text{Ca}$ . However, it is because the O shell is a convective-reactive environment where species can advect on a similar timescale to their reactions. Fig. 2 shows a build-up of  $^{43}\text{Sc}$  which is mixed deeper in the O and undergoes  $^{43}\text{Sc}(\gamma, p)^{42}\text{Ca}$  at those hotter temperatures. For  $^{38}\text{Ar}$ , in all other cases it is produced by  $^{30}\text{Si}(\alpha, \gamma)^{34}\text{S}(\alpha, \gamma)^{38}\text{Ar}$ , but in the  $50 \times D_{\text{3D-insp.}}$  mixing cases it is also produced by  $^{35}\text{Cl}(\gamma, p)^{34}\text{S}(\alpha, \gamma)^{38}\text{Ar}$  and  $^{39}\text{K}(\gamma, p)^{38}\text{Ar}$ . How  $^{30}\text{Si}$  and the light odd-Z isotopes  $^{35}\text{Cl}$  and  $^{39}\text{K}$  are produced in the O-C shell merger is discussed in Issa et al. (2025b). The importance of the  $(\alpha, \gamma)$  channels of  $^{34}\text{S}$  and  $^{38}\text{Ar}$  for  $^{44}\text{Ti}$  production are interesting as their  $(p, \gamma)$  channels may dominate energy production in the O-C shell (Roberti & Pignatari 2025).

Despite the shared chain of production, Fig. 3 shows  $^{44}\text{Ti}$  production is dependent on the mixing conditions of the merger. Only models with the highest entrainment rate of  $4 \times 10^{-3} M_{\odot}\text{s}^{-1}$  and a boosted 3D-inspired mixing profile show significant increase to the production of  $^{44}\text{Ti}$  compared to the pre-explosive production of the  $15 M_{\odot}$ ,  $Z = 0.02$  model from Ritter et al. (2018).  $^{44}\text{Ti}$  production is also monotonic with mixing speed for the 3D-inspired mixing profiles. Despite having the same entrainment rate, the MLT and quenched mixing cases show a decrease in  $^{44}\text{Ti}$  production compared to the pre-explosive model.

Entrainment of C-shell material supplies a significant source of  $^{43}\text{Ca}$  which boosts the  $^{44}\text{Sc}$ . As the mixing

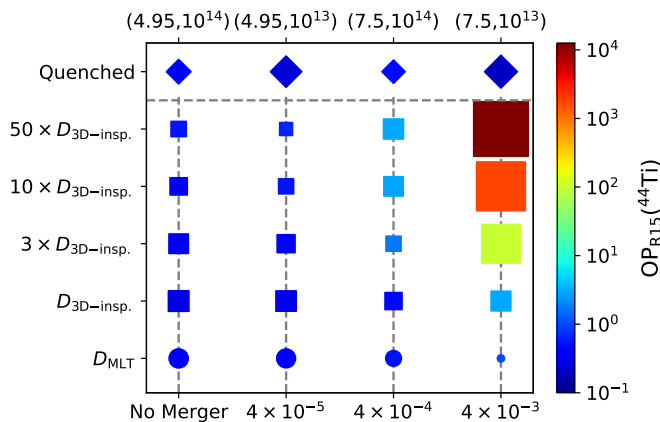


**Fig. 3.** Predicted yields of  $^{44}\text{Ti}$  compared to the  $15 \text{ M}_\odot Z = 0.02$  pre-explosive yields ( $\text{OP}_{\text{R15}}$ ). The lower x-axis has the entrainment rates in  $\text{M}_\odot \text{s}^{-1}$  and the upper x-axis has the quenched mixing cases summarized as (location of dip in  $\text{Mm}$ , maximum extent of the dip in  $\text{cm}^2 \text{s}^{-1}$ ). Colour indicates magnitude and size indicates distance from  $\text{OP}_{\text{R15}} = 1$ . The explosive production of the  $15 \text{ M}_\odot Z = 0.02$  model is  $\text{OP}_{\text{R15}} = 0.49$  dex.

speed increases, the location of the reaction peak for  $^{43}\text{Ca}(p, \gamma)^{44}\text{Sc}$  and  $^{44}\text{Sc}(p, n)^{44}\text{Ti}$  move from  $1.65 \text{ M}_\odot [T = 2.23 \times 10^9 \text{ K}]$  in the MLT case to  $1.59 \text{ M}_\odot [T = 2.56 \times 10^9 \text{ K}]$  in the  $50 \times D_{3\text{D}-\text{insp.}}$  case. The location of peak burning shifting is a feature of the convective-reactive nucleosynthesis explored in Issa et al. (2025a,b). This demonstrates the importance of both the entrainment rate and mixing speed in for pre-explosive nucleosynthesis of  $^{44}\text{Ti}$  during an O-C shell merger.

### 3.2. Mixing and explosive yields of radioactive species

Mixing potentially impacts the estimated pre-explosive yields of a broader range of radioactive isotopes produced in the O shell, beyond  $^{44}\text{Ti}$ . Fig. 4 shows the maximum and minimum yields for radioactive isotopes from our pre-explosive mixing scenarios and explosive yields from models and observations for  $^{44}\text{Ti}$ .

Fig. 4 shows that all radioactive isotopes considered in this work except  $^{26}\text{Al}$  feature a multi-dex spread in their predicted yields, with an average spread of 2.14 dex (excluding  $^{26}\text{Al}$  as it is not exclusive to the O-C merger as shown in Fig. 1). Considering only the  $15 \text{ M}_\odot, Z = 0.02$  model, Depending on the mixing conditions, the yields of  $^{22}\text{Na}$ ,  $^{44}\text{Ti}$ ,  $^{51}\text{Cr}$ , and  $^{65}\text{Zn}$  could be dominated by pre-explosive merger nucleosynthesis rather than the explosion.  $^{59}\text{Fe}$  and  $^{60}\text{Fe}$  are not dominated but could be significantly contributed to by the merger. Among the radioactive isotopes considered,  $^{44}\text{Ti}$  is the most sensitive to the mixing conditions with a spread of 4.78 dex.

The range of predicted pre-explosive yields in our mixing scenarios for  $^{22}\text{Na}$ ,  $^{44}\text{Ti}$ , and  $^{51}\text{Cr}$  are comparable or larger than the explosive yields of all massive star models in the NuGrid data set. Our pre-explosive yields of  $^{59}\text{Fe}$ ,  $^{60}\text{Fe}$ , and  $^{65}\text{Zn}$  are also comparable or larger than many of the explosive yields in the NuGrid data set. Table A.2 in Appendix A shows that explosive nucleosynthesis dominates  $^{44}\text{Ti}$  yields in the NuGrid data set except for the  $15 \text{ M}_\odot, Z = 0.02$  model and the  $20 \text{ M}_\odot, Z = 0.01$  model

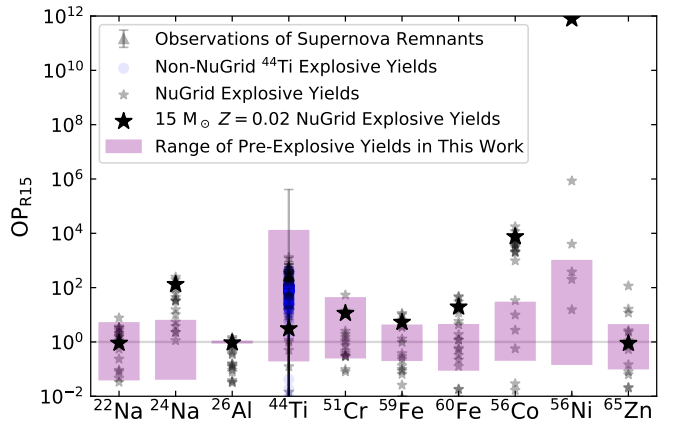


**Fig. 4.**  $\text{OP}_{\text{R15}}$  for (1) inferred yields of  $^{44}\text{Ti}$  from supernova remnants observations (triangles with error bars) (2) explosive  $^{44}\text{Ti}$  yields of non-NuGrid models (blue circles) (3) explosive yields of all considered radioactive species from NuGrid models (small black stars) (4) explosive yields of the  $15 \text{ M}_\odot Z = 0.02$  NuGrid model (large black stars) (5) the maximum and minimum predicted pre-explosive yields for all scenarios (purple bars). Appendix A provides the full list of citations.

as the only two models where pre-explosive yields of  $^{44}\text{Ti}$  are comparable to the explosion. Notably the other two models with O-C shell mergers do not show significant pre-explosive production of  $^{44}\text{Ti}$ , but could do so if 3D mixing effects were included as in this work.

We have also compared our results to a number of 1D, 2D, and 3D models of massive star yields of  $^{44}\text{Ti}$  from the literature, some of which include rotation. Fig. 4 shows that the range of predicted pre-explosive yields for  $^{44}\text{Ti}$  can dominate regardless of the different modelling assumptions and dimensionality of the explosion. Additionally, our predicted range does not exceed the inferred yields of  $^{44}\text{Ti}$  from observed supernova remnants, although the largest upper limit comes from Vela Junior which has large uncertainties in its distance and age (Weinberger et al. 2020). Even so, our results are not inconsistent with observational evidence. For instance, according to Weinberger et al. (2020) Cassiopeia A ejected  $(2.6 \pm 0.6) \times 10^{-4} \text{ M}_\odot$  of  $^{44}\text{Ti}$  which is between our  $3 \times$  and  $10 \times D_{3\text{D}-\text{insp.}}$  cases with the fastest entrainment rate of  $4 \times 10^{-3} \text{ M}_\odot \text{s}^{-1}$ . If the progenitor of Cassiopeia A underwent an O-C shell merger prior to explosion (Sato et al. 2025; Audard et al. 2025), the mixing profile of its O shell having a convective downturn and mixing speeds boosted by 3–10 compared to MLT would explain the  $^{44}\text{Ti}$  yield without much synthesis in the explosion. These results demonstrate the critical importance of understanding the mixing conditions during the O-C shell merger for predicting the yields of radioactive isotopes for pre-supernova models, especially  $^{44}\text{Ti}$ .

## 4. Conclusions

This work highlights the need to understand the 3D macro physics of mixing in the O shell during a merger. We have shown how  $^{44}\text{Ti}$  can be significantly produced by pre-explosive nucleosynthesis during an O-C shell merger in massive stars by  $^{44}\text{Sc}(p, n)^{44}\text{Ti}$  and its sensitivity to both entrainment and mixing speed. We have also found that  $^{22}\text{Na}$ ,  $^{51}\text{Cr}$ ,  $^{59,60}\text{Fe}$ , and  $^{65}\text{Zn}$  also have relevant pre-

explosive nucleosynthesis depending on the mixing conditions. Further, we have shown for  $^{44}\text{Ti}$  that the pre-explosive O-C shell production can dominate over explosive yields from a wide range of massive star models and are consistent with observations.

These predicted results do not properly account for the pre-collapse evolution of the O-C shell merger and how feedback effects may alter the final nucleosynthesis. However, this work does show the importance of including insights from 3D macro physics into 1D stellar evolution and explosion models to better understand the nucleosynthesis of radioactive isotopes in massive stars. Another feature missing from this model is a treatment of rotation as Chieffi & Limongi (2017) found it could boost pre-explosive  $^{44}\text{Ti}$  production during convective O shell burning. 3D effects of a convective downturn and boosted mixing speeds compared to MLT are general features of O shell convection (Jones et al. 2017), and our results find a spread even in the absence of a merger (left column of Fig. 3). 3D explosive effects may also complicate this picture as  $^{44}\text{Ti}$  production is boosted compared to 1D explosions (Sieverding et al. 2023). We note that both Chieffi & Limongi (2017) and Sieverding et al. (2023) results are included in Fig. 4. The relationship between mergers and the subsequent explosion need further study as the non-radial perturbations from it may also play a significant role in how the subsequent supernova explodes (Couch & Ott 2013; Müller et al. 2017; Müller 2020; Andrassy et al. 2020; Yadav et al. 2020; Fields & Couch 2020; Rizzuti et al. 2024; Laplace et al. 2025).

If the O-C merger contributes to the yields of radioactive isotopes of massive stars, then understanding the mixing conditions has a wide range of implications for observations. Supernova remnants like Cassiopeia A (Sato et al. 2025), interpretation of pre-solar grain measurements of  $^{44}\text{Ca}$  from  $^{44}\text{Ti}$  decays (Pignatari et al. 2013; Liu et al. 2024), and understanding supernova light curves powered by  $^{22}\text{Na}$  or  $^{44}\text{Ti}$  decays (Pignatari et al. 2025) are all potentially impacted by the mixing discussed in this work. Upcoming missions such as *COSI* will measure decay lines for  $^{44}\text{Ti}$  and  $^{60}\text{Fe}$ , providing more data to constrain massive star nucleosynthesis with supernova remnants (Tomsick et al. 2019). We conclude 3D hydrodynamic macro physics are a crucial part of understanding the nucleosynthesis and origin of radioactive isotopes, particularly  $^{44}\text{Ti}$ , during O-C mergers.

**Acknowledgements.** We would like to thank Marco Pignatari and Roberto Lorenzi for useful discussions and feedback. FH is supported by a Natural Sciences and Engineering Research Council of Canada (NSERC) Discovery Grant. This research has used the Astrohub online virtual research environment (<https://astrohub.uvic.ca>), developed and operated by the Computational Stellar Astrophysics group at the University of Victoria and hosted on the Digital Research Alliance of Canada Arbutus Cloud at the University of Victoria. These simulations were performed on Digital Research Alliance's Niagara supercomputer cluster operated by SciNet at the University of Toronto. This work benefited from interactions and workshops co-organized by The Center for Nuclear astrophysics Across Messengers (CeNAM) which is supported by the U.S. Department of Energy, Office of Science, Office of Nuclear Physics, under Award Number DE-SC0023128.

Audard, M., Awaki, H., Ballhausen, R., et al. 2025, *Nature Astronomy*, 1

Boggs, S. E., Harrison, F. A., Miyasaka, H., et al. 2015, *Science*, 348, 670

Borkowski, K. J., Reynolds, S. P., Green, D. A., et al. 2010, *The Astrophysical Journal Letters*, 724, L161

Chieffi, A. & Limongi, M. 2017, *The Astrophysical Journal*, 836, 79

Couch, S. M. & Ott, C. D. 2013, *The Astrophysical Journal*, 778, L7

Eichler, M., Nakamura, K., Takiwaki, T., et al. 2017, *Journal of Physics G: Nuclear and Particle Physics*, 45, 014001

Fields, C. E. & Couch, S. M. 2020, *The Astrophysical Journal*, 901, 33

Fryer, C. L., Belczynski, K., Wiktorowicz, G., et al. 2012, *The Astrophysical Journal*, 749, 91

Grebenev, S. A., Lutovinov, A. A., Tsygankov, S. S., & Winkler, C. 2012, *Nature*, 490, 373

Grefenstette, B. W., Fryer, C. L., Harrison, F. A., et al. 2017, *The Astrophysical Journal*, 834, 19

Grefenstette, B. W., Harrison, F. A., Boggs, S. E., et al. 2014, *Nature*, 506, 339

Issa, J., Herwig, F., Denissenkov, P., & Pignatari, M. 2025a, *Impact of 3D Macro Physics and Nuclear Physics on the p Nuclei in O-C Shell Mergers*

Issa, J., Herwig, F., Mojzsis, S. J., & Pignatari, M. 2025b, *3D Macro Physics and Light Odd-Z Element Production in O-C Shell Mergers: Implications for  $\mathcal{K}$  Production and Radioactive Heating Inventories of Rocky Exoplanets*

Iyudin, A. F., Diehl, R., Bloemen, H., et al. 1994, *Astronomy and Astrophysics*, 284, L1

Jerkstrand, A., Fransson, C., & Kozma, C. 2011, *Astronomy & Astrophysics*, 530, A45

Jones, S., Andrassy, R., Sandalski, S., et al. 2017, *Monthly Notices of the Royal Astronomical Society*, 465, 2991

Laplace, E., Schneider, F. R. N., & Podsiadlowski, P. 2025, *Astronomy & Astrophysics*, 695, A71

Liu, N., Lugaro, M., Leitner, J., Meyer, B. S., & Schönbaechler, M. 2024, *Space Science Reviews*, 220, 88

Magkotsios, G., Timmes, F. X., Hungerford, A. L., et al. 2010, *The Astrophysical Journal Supplement Series*, 191, 66

Meakin, C. A. & Arnett, D. 2006, *The Astrophysical Journal*, 637, L53

Müller, B. 2020, *Living Reviews in Computational Astrophysics*, 6, 3

Müller, B., Melson, T., Heger, A., & Janka, H.-T. 2017, *Monthly Notices of the Royal Astronomical Society*, 472, 491

Paxton, B., Bildsten, L., Dotter, A., et al. 2010, *The Astrophysical Journal Supplement Series*, 192, 3

Pignatari, M., Amari, S., Hoppe, P., et al. 2025, *The Astrophysical Journal*, 990, 19

Pignatari, M., Herwig, F., Hirschi, R., et al. 2016, *The Astrophysical Journal Supplement Series*, 225, 24

Pignatari, M., Wiescher, M., Timmes, F. X., et al. 2013, *The Astrophysical Journal Letters*, 767, L22

Ritter, C., Herwig, F., Jones, S., et al. 2018, *Astronomy & Astrophysics*, 615

Rizzuti, F., Hirschi, R., Varma, V., et al. 2024, *Monthly Notices of the Royal Astronomical Society*, 533, 687

Robert, L. & Pignatari, M. 2025, *Astronomy and Astrophysics*, 703, L15

Robert, L., Pignatari, M., Brinkman, H. E., et al. 2025, *Astronomy and Astrophysics*, 698, A216

Sato, T., Matsumaga, K., Uchida, H., et al. 2025, *The Astrophysical Journal*, 990, 103

Siegert, T., Diehl, R., Krause, M. G. H., & Greiner, J. 2015, *Astronomy & Astrophysics*, 579, A124

Sieverding, A., Kresse, D., & Janka, H.-T. 2023, *The Astrophysical Journal*, 957, L25

Sukhbold, T., Ertl, T., Woosley, S. E., Brown, J. M., & Janka, H.-T. 2016, *The Astrophysical Journal*, 821, 38

The, L.-S., Clayton, D. D., Diehl, R., et al. 2006, *Astronomy and Astrophysics*, 450, 1037

Tomsick, J., Zoglauer, A., Sleator, C., et al. 2019, *The Compton Spectrometer and Imager*

Troja, E., Segreto, A., La Parola, V., et al. 2014, *The Astrophysical Journal Letters*, 797, L6

Vink, J., Laming, J. M., Kaastra, J. S., et al. 2001, *The Astrophysical Journal*, 560, L79

Wang, W. & Li, Z. 2016, *The Astrophysical Journal*, 825, 102

Weinberger, C., Diehl, R., Pleintinger, M. M. M., Siegert, T., & Greiner, J. 2020, *Astronomy and Astrophysics*, 638, A83

Wongwathanarat, A., Janka, H. T., Müller, E., Pliumbi, E., & Wanajo, S. 2017, *Astrophysical Journal*, 842, 13

Woosley, S. E. & Weaver, T. A. 1995, *The Astrophysical Journal Supplement Series*, 101, 181

Yadav, N., Müller, B., Janka, H. T., Melson, T., & Heger, A. 2020, *The Astrophysical Journal*, 890, 94

## References

Andrassy, R., Herwig, F., Woodward, P., & Ritter, C. 2020, *Monthly Notices of the Royal Astronomical Society*, 491, 972

## Appendix A: $^{44}\text{Ti}$ Yields

Here we provide a full list of citations for the yields of  $^{44}\text{Ti}$  shown in Fig. 4. Table A.1 is the predicted pre-explosive  $^{44}\text{Ti}$  yields from this work that are calculated according to the method described in Issa et al. (2025b). Table A.2 provides the pre-explosive and explosive  $^{44}\text{Ti}$  yields from the massive stars from the NuGrid data set (Pignatari et al. 2016; Ritter et al. 2018) using the delayed explosion mass cut from Fryer et al. (2012). Table A.3 is the selection of 1D, 2D, and 3D models from the literature that report explosive  $^{44}\text{Ti}$  yields. Finally, Table A.4 is a list of inferred  $^{44}\text{Ti}$  yields from observed supernova remnants in the literature.

**Table A.1.** Predicted pre-explosive  $^{44}\text{Ti}$  yields from the Issa et al. (2025a,b) models.

Mixing Profile	Ingestion Rate ( $\text{M}_\odot \text{ s}^{-1}$ )	Predicted $^{44}\text{Ti}$ Yield ( $\text{M}_\odot$ )
$D_{\text{MLT}}$	0	$1.94 \times 10^{-7}$
$D_{\text{MLT}}$	$4 \times 10^{-5}$	$2.00 \times 10^{-7}$
$D_{\text{MLT}}$	$4 \times 10^{-4}$	$2.83 \times 10^{-7}$
$D_{\text{MLT}}$	$4 \times 10^{-3}$	$5.40 \times 10^{-7}$
$D_{\text{3D-inspired}}$	0	$1.61 \times 10^{-7}$
$D_{\text{3D-inspired}}$	$4 \times 10^{-5}$	$1.66 \times 10^{-7}$
$D_{\text{3D-inspired}}$	$4 \times 10^{-4}$	$2.46 \times 10^{-7}$
$D_{\text{3D-inspired}}$	$4 \times 10^{-3}$	$1.60 \times 10^{-6}$
$3 \times D_{\text{3D-inspired}}$	0	$1.85 \times 10^{-7}$
$3 \times D_{\text{3D-inspired}}$	$4 \times 10^{-5}$	$2.22 \times 10^{-7}$
$3 \times D_{\text{3D-inspired}}$	$4 \times 10^{-4}$	$9.54 \times 10^{-7}$
$3 \times D_{\text{3D-inspired}}$	$4 \times 10^{-3}$	$5.65 \times 10^{-5}$
$10 \times D_{\text{3D-inspired}}$	0	$2.40 \times 10^{-7}$
$10 \times D_{\text{3D-inspired}}$	$4 \times 10^{-5}$	$3.03 \times 10^{-7}$
$10 \times D_{\text{3D-inspired}}$	$4 \times 10^{-4}$	$1.53 \times 10^{-6}$
$10 \times D_{\text{3D-inspired}}$	$4 \times 10^{-3}$	$9.83 \times 10^{-4}$
$50 \times D_{\text{3D-inspired}}$	0	$2.96 \times 10^{-7}$
$50 \times D_{\text{3D-inspired}}$	$4 \times 10^{-5}$	$3.66 \times 10^{-7}$
$50 \times D_{\text{3D-inspired}}$	$4 \times 10^{-4}$	$1.67 \times 10^{-6}$
$50 \times D_{\text{3D-inspired}}$	$4 \times 10^{-3}$	$6.69 \times 10^{-3}$
Quenched at 4.95 Mm to $10^{14} \text{ cm}^2 \text{s}^{-1}$	$4 \times 10^{-3}$	$2.38 \times 10^{-7}$
Quenched at 4.95 Mm to $10^{13} \text{ cm}^2 \text{s}^{-1}$	$4 \times 10^{-3}$	$1.29 \times 10^{-7}$
Quenched at 7.5 Mm to $10^{14} \text{ cm}^2 \text{s}^{-1}$	$4 \times 10^{-3}$	$2.61 \times 10^{-7}$
Quenched at 7.5 Mm to $10^{13} \text{ cm}^2 \text{s}^{-1}$	$4 \times 10^{-3}$	$1.10 \times 10^{-7}$

**Table A.2.** Pre-explosive and explosive  $^{44}\text{Ti}$  yields of the Ritter et al. (2018) models.

Mass	Metallicity	Pre-Explosive Yield ( $\text{M}_\odot$ )	Explosive Yield ( $\text{M}_\odot$ )	O-C Merger
12	0.0001	$3.74 \times 10^{-9}$	$1.25 \times 10^{-4}$	
12	0.001	$2.41 \times 10^{-9}$	$6.30 \times 10^{-5}$	
12	0.006	$2.62 \times 10^{-9}$	$1.09 \times 10^{-4}$	
12	0.01	$5.02 \times 10^{-9}$	$1.02 \times 10^{-4}$	Yes
12	0.02	$3.51 \times 10^{-9}$	$8.37 \times 10^{-5}$	
15	0.0001	$1.93 \times 10^{-10}$	$8.39 \times 10^{-6}$	
15	0.001	$1.75 \times 10^{-11}$	$4.14 \times 10^{-6}$	
15	0.006	$2.13 \times 10^{-10}$	$6.16 \times 10^{-5}$	
15	0.01	$1.69 \times 10^{-9}$	$7.36 \times 10^{-6}$	Yes
15	0.02	$5.36 \times 10^{-7}$	$1.65 \times 10^{-6}$	Yes
20	0.0001	$3.70 \times 10^{-12}$	$5.19 \times 10^{-7}$	
20	0.001	$3.83 \times 10^{-11}$	$5.97 \times 10^{-6}$	
20	0.006	$1.49 \times 10^{-11}$	$6.88 \times 10^{-4}$	
20	0.01	$2.67 \times 10^{-7}$	$2.67 \times 10^{-7}$	Yes
20	0.02	$2.55 \times 10^{-11}$	$6.17 \times 10^{-7}$	
25	0.0001	$2.41 \times 10^{-14}$	$4.64 \times 10^{-11}$	
25	0.001	$2.05 \times 10^{-13}$	$6.64 \times 10^{-8}$	
25	0.006	$3.26 \times 10^{-13}$	$4.44 \times 10^{-9}$	
25	0.01	$4.23 \times 10^{-13}$	$5.21 \times 10^{-6}$	
25	0.02	$1.32 \times 10^{-11}$	$7.72 \times 10^{-9}$	

**Table A.3.** Explosive  $^{44}\text{Ti}$  yields from models in the literature.

Paper	$^{44}\text{Ti}$ Yield ( $\text{M}_\odot$ )	Notes
Woosley & Weaver (1995)	$1.35 \times 10^{-33} - 2.44 \times 10^{-4}$	1D Models ( $11-40 \text{ M}_\odot, 0-1 \text{ Z}_\odot$ )
Magkotsios et al. (2010)	$1.04 \times 10^{-4}$	1D Supernova ( $16 \text{ M}_\odot, \text{Z}_\odot$ )
	$2.66 \times 10^{-5}$	1D Hypernova ( $16 \text{ M}_\odot, \text{Z}_\odot$ )
	$6.98 \times 10^{-5}$	2D Rotating Supernova ( $15 \text{ M}_\odot, \text{Z}_\odot$ )
Sukhbold et al. (2016) <sup>a</sup>	$(0-7.45) \times 10^{-5}$	1D Neutrino-Driven Supernovae ( $9-120 \text{ M}_\odot, \text{Z}_\odot$ )
Chieffi & Limongi (2017)	$(0.89-6.0) \times 10^{-5}$	1D Non-Rotating Models ( $13-120 \text{ M}_\odot, [\text{Fe}/\text{H}] = -1, 0$ )
	$(0.6-5.8) \times 10^{-5}$	1D Rotating Models ( $13-120 \text{ M}_\odot, [\text{Fe}/\text{H}] = -1, 0$ )
Eichler et al. (2017)	$(1.14-1.35) \times 10^{-5}$	2D Supernova ( $17 \text{ M}_\odot, \text{Z}_\odot$ )
Wongwathanarat et al. (2017)	$8.66 \times 10^{-6} - 1.49 \times 10^{-4}$	3D Neutrino-Driven Supernova ( $15 \text{ M}_\odot, \text{Z}_\odot$ )
Sieverding et al. (2023)	$1.80 \times 10^{-5}$	3D Neutrino-Driven Supernova ( $18.88 \text{ M}_\odot, \text{Z}_\odot$ )

**Notes.** <sup>(a)</sup> Yields for this work are from <http://doi.org/10.17617/1.b>.

**Table A.4.**  $^{44}\text{Ti}$  yields from observations in the literature.

Paper	Inferred $^{44}\text{Ti}$ Yield ( $\text{M}_\odot$ )	Notes
Iyudin et al. (1994)	$(1.4 \pm 0.4) \times 10^{-4}$	Cassiopeia A
	$(3.2 \pm 0.8) \times 10^{-4}$	
Vink et al. (2001)	$(0.8-2.5) \times 10^{-4}$	Cassiopeia A
Borkowski et al. (2010)	$2.8_{-1.7}^{+2.3} \times 10^{-5}$	G1.9+0.3 <sup>a</sup>
	$1.3_{-0.94}^{+1.3} \times 10^{-5}$	
	$3.3_{-2.35}^{+3.2} \times 10^{-5}$	
Jerkstrand et al. (2011)	$(1.5 \pm 0.5) \times 10^{-4}$	SN 1987A
Grebenev et al. (2012)	$(3.1 \pm 0.8) \times 10^{-4}$	SN 1987A
Troja et al. (2014)	$(0.3-3) \times 10^{-4}$	Tycho's SNR <sup>a</sup>
Boggs et al. (2015)	$(1.5 \pm 0.3) \times 10^{-4}$	SN 1987A
Siegert et al. (2015)	$(1.37 \pm 0.19) \times 10^{-4}$	Cassiopeia A
Wang & Li (2016)	$(1.3 \pm 0.4) \times 10^{-4}$	Cassiopeia A
Grefenstette et al. (2017)	$(1.54 \pm 0.21) \times 10^{-4}$	Cassiopeia A
Weinberger et al. (2020)	$2.6 \pm 0.6 \times 10^{-4}$	Cassiopeia A
	$\leq 6.9 \times 10^{-4}$	SN 1987A
	$\leq 3.3 \times 10^{-5}$ or $\leq 2.2 \times 10^{-1}$	Vela Junior <sup>b</sup>
	$\leq 4.8 \times 10^{-4}$	Tycho's SNR <sup>a</sup>
	$\leq 3 \times 10^{-5}$	G1.9E+0.3 <sup>a</sup>
	$\leq 4 \times 10^{-4}$	Kepler's SNR <sup>a</sup>

**Notes.** <sup>(a)</sup> Thought to be a Type Ia supernova remnant. <sup>(b)</sup> Unknown supernova type.